Catalysis Today 364 (2021) 196–201

Contents lists available at ScienceDirect

Catalysis Today

journal homepage: www.elsevier.com/locate/cattod

Towards anti-perovskite nitrides as potential nitrogen storage materials for chemical looping ammonia production: Reduction of Co_3ZnN, Ni_3ZnN, Co_3InN and Ni_3InN under hydrogen

Y. Goto, A. Daisley, J.S.J. Hargreaves *

WestCHEM, School of Chemistry, Joseph Black Building, University of Glasgow, G12 8QQ, United Kingdom

ARTICLE INFO

Keywords:
Anti-perovskite nitride
Nitrogen storage material
Chemical looping ammonia production
Topotactic reaction

ABSTRACT

The ammonia production properties upon reduction in hydrogen of the anti-perovskite nitrides Co_3ZnN, Ni_3ZnN, Co_3InN, and Ni_3InN have been investigated. Single phases with ideal anti-perovskite structures (Space group: *Pm-3m*) were prepared for all the nitrides by the ammonolysis of the corresponding precursor oxides and all the nitrides were observed to produce ammonia in high yields when reacted with H_2/Ar. The cumulative ammonia production values at 400 °C were 3069, 2925, 289, and 1029 μmol-NH_3 g^{-1} for Co_3ZnN, Ni_3ZnN, Co_3InN, and Ni_3InN, respectively and the order of the release rates was Ni_3ZnN > Co_3ZnN > Ni_3InN > Co_3InN. X-ray diffraction studies revealed that Co_3ZnN and Co_3InN decomposed upon the loss of lattice N, whereas Ni_3ZnN and Ni_3InN were transformed into Ni_3Zn and Ni_3In via the intermediate phases Ni_3ZnN_x and Ni_3InN_y. The crystal structures of these intermediate phases are related to their initial structures, indicating that the loss of lattice N in Ni_3ZnN and Ni_3InN was topotactic.

1. Introduction

Ammonia production, currently accomplished on the industrial scale via the Haber-Bosch Process, is a reaction of pivotal societal importance [1]. It can be credited with the sustenance of around 40 % of the global population through the provision of an accessible route to synthetic fertilizer. Around 174 million tonnes of ammonia are produced on the industrial scale annually [1] and production continues to grow. When considered in its entirety, including the production of the feedstream reagents, the Haber-Bosch Process currently accounts for around 1–2 % of global energy demand [1]. The hydrogen required is generated currently from fossil sources and the process has been reported to be responsible for the production of about 2.5 % of all fossil fuel based CO_2 emissions worldwide [1]. Accordingly, in view of the paramount importance of this reaction, recent studies have sought to address issues of sustainability. One topic of focus has been the possibility of the development of ammonia synthesis technology which would be suitable for operation on a local scale, being much smaller than the traditional Haber-Bosch plants which are operated on a large scale, where, for example, the local generation of fertilizer on a farm could be accomplished using hydrogen generated via electrolysis employing renewably derived energy such as that from wind power. In order to accomplish this, using heterogeneous catalysis, a step change in catalyst performance is necessary and, correspondingly, the development of new catalysts of enhanced performance with respect to the industrially employed iron-based [2] and ruthenium based [3] catalysts is an area of contemporary interest. It is widely believed that in order to achieve this, the limiting scaling relationship which has been reported for ammonia synthesis will need to be broken. Amongst catalysts investigated to date have been electride supported metals in which novel mechanistic pathways are reported to be operative [4], the combination of lithium hydride and metals or metal nitrides which are proposed to circumvent scaling limitations via the transfer of reaction intermediates between phases [5], ternary [6,7] and quaternary [8] metal nitrides which might operate by nitrogen based Mars-van Krevelen mechanisms [9,10] and hydride and metal hydride based compositions [11,12] for which hydrogen based Mars-van Krevelen mechanisms may be operational. In addition to the development of novel, more active, heterogeneous catalysts, photocatalytic [13] and electrocatalytic [14,15] processes have also been investigated.

A further approach which has been of interest in the context of localised ammonia synthesis involves chemical looping in which production is accomplished via the reaction of a nitrogen containing reagent followed by its regeneration in a separate reaction step. A number

* Corresponding author.
E-mail address: Justin.Hargreaves@glasgow.ac.uk (J.S.J. Hargreaves).

https://doi.org/10.1016/j.cattod.2020.03.022
Received 20 December 2019; Received in revised form 26 February 2020; Accepted 13 March 2020
Available online 16 March 2020

of these studies have employed the hydrolysis of a nitride followed by its regeneration at high temperature employing N_2, e.g. [16,17]. It has been reported that the high temperatures required for renitridation could be accomplished from solar energy. By such routes, ammonia production from nitrogen, water and sunlight becomes possible making it entirely sustainable with a dramatically reduced carbon footprint. Related to this has been the report of a system for ammonia synthesis based upon hydrolysis of lithium nitride and its subsequent regeneration by electrochemical means [18]. Whilst it is less direct, the possible availability of sustainable hydrogen derived from water, means that looping approaches based upon hydrogenation of regenerable metal nitrides is also an area of interest. Accordingly, reports have been made of ammonia production via the hydrogenation of systems based upon binary metal nitrides including Re_3N [19], Ni_3N [20], Cu_3N [20], Zn_3N_2 [20] Ta_3N_5 [20,21] and manganese nitride [22] have been reported. In the current study, we extend these studies towards anti-perovskite nitrides (general formula A_3BN, see Fig. 1 for their structure) which offer the possibility of tuning the reactivity of lattice nitrogen and regeneration via the controlled variation of the metal (i.e. A and B site) composition. The aim of this work is to establish composition – performance relationships which might also prove to be of value for for the computationally aided design of more active heterogeneous catalysts [23]. In the current study, we report the lattice nitrogen hydrogenation characteristics of cobalt, nickel, zinc and indium based anti-perovskite nitrides. It is of interest to note that the removal and replenishment of lattice nitrogen from anti-perovskite nitrides is in some way analogous to the exsolution of metal nanoparticles from perovskites which is an area of topical interest [24]. Also of relevance to the approach reported within the current manuscript are reports of the nitrogenation and hydrogenation characteristics of transition metal – iron intermetallic compounds [25] and the nitrogen absorption behaviour of zirconium vanadium iron and related alloys [26].

2. Experimental details

2.1. Sample preparation

Polycrystalline samples of Co_3ZnN, Ni_3ZnN, Co_3InN, and Ni_3InN were synthesized by ammonolysis of precursor oxides which in turn were prepared from nitrate solutions. Stoichiometric amounts of Co $(NO_3)_2{\cdot}6H_2O$ (98.0 – 102.0 %, Alfa Aesar), $Ni(NO_3)_2{\cdot}6H_2O$ (≥98 %, Fluka), $Zn(NO_3)_2{\cdot}6H_2O$ (≥99.0 %, Sigma Aldrich), and $In(NO_3)_3{\cdot}xH_2O$ (99.99 %, Alfa Aesar) were dissolved in a minimal amount of HNO_3 aqueous solution (10 %) and stirred at room temperature for 30 min. The solution was dried at 120 °C overnight, followed by calcination in air at 400 °C for 3 h. The precursor oxides obtained were nitrided under a flow of NH_3 (99.98 %, BOC, 95 mL min^{-1}) at 600 °C for 10 h employing a ramp rate of 2.5 °C min^{-1}, followed by subsequent cooling to room temperature under the flow of NH_3. The obtained nitrides were subsequently passivated applying a flow of 0.1 % O_2/N_2/Ar (prepared by mixing 2% O_2/Ar and 99.998 % N_2, BOC, 100 mL min^{-1}) at room temperature for 5 h in order to prevent bulk oxidation upon discharging samples from the reactor.

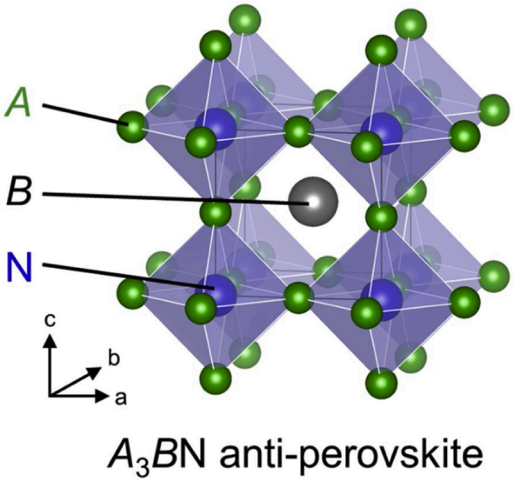

Fig. 1. Crystal structure of A_3BN anti-perovskite with the space group of *Pm*-3*m*. The green, gray, and blue spheres represent atoms in *A* site, atoms in *B* site, and N atoms, respectively (For interpretation of the references to colour in this figure legend, the reader is referred to the web version of this article).

2.2. Characterization

Powder X-ray diffraction (XRD) measurements were conducted using an X'Pert PRO MPD (PANalytical) employing Cu Kα radiation (λ =1.54056 Å). XRD patterns were collected in the 2θ 20 – 85° range with a step size of 0.0167°. Le Bail refinements for the XRD patterns obtained were performed using the Jana2006 program [27] with a pseudo-Voigt function in order to estimate lattice parameters. Energy dispersive X-ray spectroscopy (EDX) was collected using a XL30 ESEM (Philips/FEI) at an accelerating voltage of 20 kV. Specific surface areas were determined by Brunauer Emmett Teller (BET) analysis of 20 point nitrogen physisorption isotherms determined at −196 °C using a Quantachrome Quadrasorb Evo Analyser. Prior to measurements being undertaken, samples were degassed at 120 °C for 16 h under vacuum. N and H content analyses were conducted by combustion using an CE-440 Elemental Analyser (Exeter Analytical).

2.3. Evaluation of ammonia production

Samples (0.2 g) were placed inside quartz microreactor tubes and were held in place centrally between quartz wool plugs and housed in a Carbolite tube furnace. Samples were heated under a flow of H_2/Ar (75 % H_2, BOC, 60 mL min^{-1}) from room temperature to the target reaction temperature (400 or 500 °C) employing a ramp rate of 10 °C min^{-1}. Samples were held for 6 h at the target temperature. The vent gas was flowed through 210 mL of H_2SO_4 solution (0.00108 M) and the change in conductivity was related to the production of NH_3.

3. Results and discussion

The XRD patterns of the precursor oxides for Co_3ZnN (Co-*Zn*-O), Ni_3ZnN (Ni-Zn-O), Co_3InN (Co-In-O), and Ni_3InN (Ni-In-O) are presented in Fig. 2. Co-Zn-O exhibited a cubic phase related to Co_3O_4, although the lattice parameter based on the *Fd*-3*m* space group was a =8.0971(7) Å, which is larger than the a=8.065 Å of Co_3O_4 [28] and which is indicative of Co-ZnO being $Co_{3-\delta}Zn_\delta O_4$ since the increase of

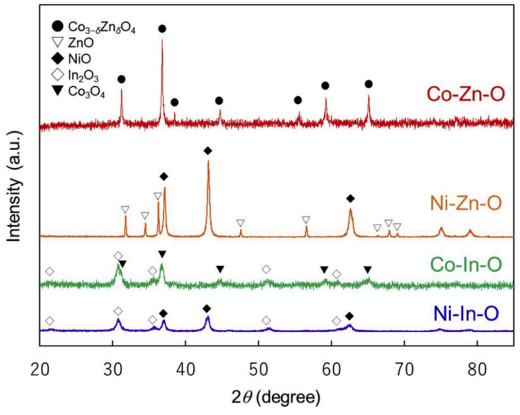

Fig. 2. XRD patterns of precursor oxides Co-Zn-O, Ni-Zn-O, Co-In-O, and Ni-In-O.

lattice parameter with respect to Co_3O_4 is consistent with Zn substitution into the lattice [29]. The value of δ based on Vegard's law was determined to be 0.85, which is in reasonable agreement with the synthesis value of $\delta = 0.75$. The other precursor oxides, Ni-Zn-O, Co-In-O and Ni-In-O were found to be mixtures comprising NiO and ZnO, Co_3O_4 and In_2O_3, and NiO and In_2O_3, respectively.

All of the XRD patterns of the samples Co_3ZnN, Ni_3ZnN, Co_3InN, and Ni_3InN showed the expected cubic phase without any additional impurity phases being present (Fig. 3). The estimated lattice parameters (Table 1) based on the ideal anti-perovskite structure with the space group of *Pm*-3*m* were all in close agreement with the reported values of a =3.764 Å for Co_3ZnN, a =3.766 Å for Ni_3ZnN, a = 3.8541(7) Å for Co_3InN, and a = 3.8445(1) Å for Ni_3InN [30–32] The N contents of Co_3ZnN, Ni_3ZnN, and Ni_3InN as determined by elemental analysis (Table 1) were also consistent with the expected values based on the A_3BN composition (A = Co Ni, B = Zn, In), although the N content of Co_3InN was approximately 10 % higher than that of theoretical value. Hydrogen, which could potentially be incorporated into the samples during the ammonolysis procedure, was not detected for any of the nitrides by combustion analysis. A/B molar ratios of Co_3ZnN, Ni_3ZnN, and Ni_3InN estimated by EDX analysis were close to the synthesis ratio of 3 for all nitrides although, as for the N analysis, that of Co_3InN was higher than expected. One possibility is that In in Co_3InN might have been partially lost during synthesis since the melting point of In metal (157 °C) is much lower than the temperature of the ammonolysis reaction (600 °C) and this requires further investigation. The surface areas of Co_3ZnN, Ni_3ZnN, Co_3InN, and Ni_3InN were found to be 3, 5, 4, and 3 m^2 g^{-1}, respectively (Table 1).

Ammonia production under 75 % H_2/Ar was investigated in order to determine the reactivity of the lattice N in these nitrides. The ammonia production profiles are presented in Fig. 4. All of the nitrides were found to produce ammonia and the production amounts at 400 °C were 3069, 2925, 289, and 1029 μmol-NH_3 g^{-1} for Co_3ZnN, Ni_3ZnN, Co_3InN, and Ni_3InN, respectively (Fig. 4a and Table 2). The nitrides did not complete ammonia production within 6 h at 400 °C. On the other hand, all of the nitrides except for Co_3InN completed ammonia production in 6 h at 500 °C (Fig. 4b) which is consistent with their post-reaction N analysis (Table 1). The production amounts at 500 °C were 3491, 3461, 1523, and 2804 μmol-NH_3 g^{-1} for Co_3ZnN, Ni_3ZnN, Co_3InN, and Ni_3InN, respectively (Fig. 4b and Table 2). These values are generally higher than for Li-Mn-N (2072 μmol-NH_3 g^{-1} for 5 h at 500 °C) [22]. Furthermore, these production amounts correspond to the consumption of 93, 92, 42, and 85 % of the total available N content of the samples respectively. These values are *ca.* 1.7–3.9 times higher than the reported values for Li-Mn-N (24 % for 5 h at 500 °C) [22].

Significant differences amongst the nitrides were observed in terms of their ammonia production rates which, estimated from the production amount in 30 min after the temperature reached 400 °C, were 752, 2082, 61, and 220 μmol-NH_3 g^{-1} h^{-1} for Co_3ZnN, Ni_3ZnN, Co_3InN, and Ni_3InN, respectively. These values do not correspond to initial production since small amounts of ammonia (1–6 % against theoretical maximum) were produced from these nitrides during the temperature increase. The ammonia production rates of the Ni-containing nitrides were *ca.* 2.8–3.6 times higher than the corresponding Co-containing nitrides and the Zn-containing nitrides were 9.5–12.3 times higher than the corresponding In-containing nitrides. The highest ammonia production rate observed for Ni_3ZnN (2082 μmol-NH_3 g^{-1} h^{-1}) was *ca.* 3.2 times higher than the catalytic ammonia production under 75 % H_2/N_2 Co_3Mo_3N (652 μmol-NH_3 g^{-1} h^{-1} at 400 °C under 0.1 MPa) [33]. N balance calculations based upon the elemental analyses reported in Table 1 and the total ammonia production reported in Table 2 are indicative of the vast majority of the lost lattice N producing NH_3 with the contribution of N_2 formation potentially being much less significant. In most instances lattice and ammonia balances are within ca. 10 % of the total, with the notable exception of the Co_3InN system where, for example, post-reaction N analyses may be influenced by oxidation of materials following their exposure to air.

The post-400 °C reaction XRD pattern of Co_3ZnN (hereafter A_3BN samples reacted at T °C are referred to as A_3BN-T) showed the presence of ZnO and Co metal in addition to unreacted Co_3ZnN (Fig. 5a), meaning that Co_3ZnN decomposed into Zn metal and Co metal upon the loss of lattice N. Unreacted Co_3ZnN was not observed in the Co_3ZnN-500 XRD pattern. ZnO was most probably formed during post-reaction exposure to air since Zn metal is easily oxidized in air even at room temperature [34]. Decomposition into Zn_3N_2 followed by subsequent oxidation to ZnO seems unrealistic because the *ca.* 93 % and 94 % of the N lost was related to ammonia production at 400 and 500 °C, respectively. In contrast, the XRD pattern of Ni_3ZnN-400 exhibited Ni_3Zn (*Fm*-3*m*) [35] and an unknown phase (denoted by α in Fig. 5a). The unknown phase is likely to be an intermediate phase such as Ni_3ZnN_x (a = 3.6630(3) Å) since its space group is the same as Ni_3ZnN (*Pm*-3*m*). The existence of an intermediate phase whose crystal structure is same as Ni_3ZnN indicates the release of lattice N to be topotactic. Since such a topotactic reaction does not require additional energy corresponding to the rearrangement of the component metal species, Ni_3ZnN showed a higher ammonia production rate than Co_3ZnN at 400 °C. The XRD pattern of Ni_3ZnN-500 showed only the single phase of Ni_3Zn, corresponding to the complete loss of lattice N from Ni_3ZnN at 500 °C.

A similar explanation for the ammonia production rate can be applied for the relation between Ni_3InN and Co_3InN. The XRD pattern of Co_3InN-400 evidenced Co metal and unreacted Co_3InN (Fig. 5b). In addition to these phases, $CoIn_2$ [36] was also detected in the XRD pattern of Co_3InN-500. These observations mean that Co_3InN decomposed into Co metal and $CoIn_2$ upon the loss of lattice N. In contrast, the XRD pattern of Ni_3InN-400 showed unreacted Ni_3InN, a small amount of Ni metal, and an unknown phase (denoted as β in Fig. 5b). The unknown phase is likely to be an intermediate phase such as Ni_3InN_y (a = 3.78394 (18) Å) which has the same space group as Ni_3InN (*Pm*-3*m*). As for Ni_3ZnN, Ni_3InN topotactically released N atoms upon initial reaction to form an intermediate phase Ni_3InN_y. This could be the reason that the ammonia release rate of Ni_3InN was higher than Co_3InN at 400 °C. The XRD pattern of Ni_3InN-500 showed Ni_3In (*P*6$_3$/*mmc*) [37] with small amount of Ni metal, consistent with the complete loss of N from Ni_3InN at 500 °C.

The 9.5 times higher ammonia rate of Ni_3ZnN compared to Ni_3InN at 400 °C cannot be explained solely on the basis of comparative surface areas (Table 1) since the area of Ni_3ZnN is less than twice that of Ni_3InN (Table 1) and SEM investigation of all the materials investigated (Figure S1 in the Supplementary Information) demonstrates them to have quite irregular morphology. Ammonia production by nitrides under the H_2/Ar atmosphere is assumed to proceed through a Mars-van Krevelen like mechanism [21,22], which comprises surface reactions and bulk diffusion of N atoms. Regarding the surface reactions, adsorption and dissociation of hydrogen molecules to produce H species,

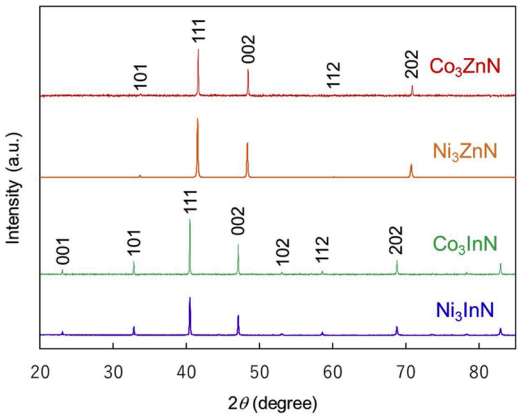

Fig. 3. XRD patterns of as prepared Co_3ZnN, Ni_3ZnN, Co_3InN, and Ni_3InN.

Table 1
Physical characteristics of the A_3BN anti-perovskite nitrides.

Compound	Lattice parameter[a] (Å)	N content[b] (wt%)				A/B molar ratio[d]	SSA[e] ($m^2\ g^{-1}$)
		Theoretical[c]	As prepared	Post reacted at 400 °C	Post reacted at 500 °C		
Co_3ZnN	3.7585(2)	5.47	5.28 ± 0.03	0.66 ± 0.01	0.06 ± 0.01	3.40 ± 0.20	3
Ni_3ZnN	3.76481(8)	5.48	5.30 ± 0.03	1.21 ± 0.01	0.03 ± 0.01	3.27 ± 0.14	5
Co_3InN	3.85672(8)	4.58	5.07 ± 0.08	4.04 ± 0.02	2.09 ± 0.02	3.70 ± 0.50	4
Ni_3InN	3.85830(6)	4.59	4.61 ± 0.01	2.72 ± 0.02	0.05 ± 0.01	3.36 ± 0.08	3

[a] Calculated on the basis of the ideal cubic perovskite structure (Space group: *Pm*-3*m*; $Z = 1$).
[b] Determined by elemental analysis.
[c] Estimated on the basis of A_3BN composition (A = Co Ni, B = Zn, In).
[d] Evaluated by EDX.
[e] Evaluated by BET analysis.

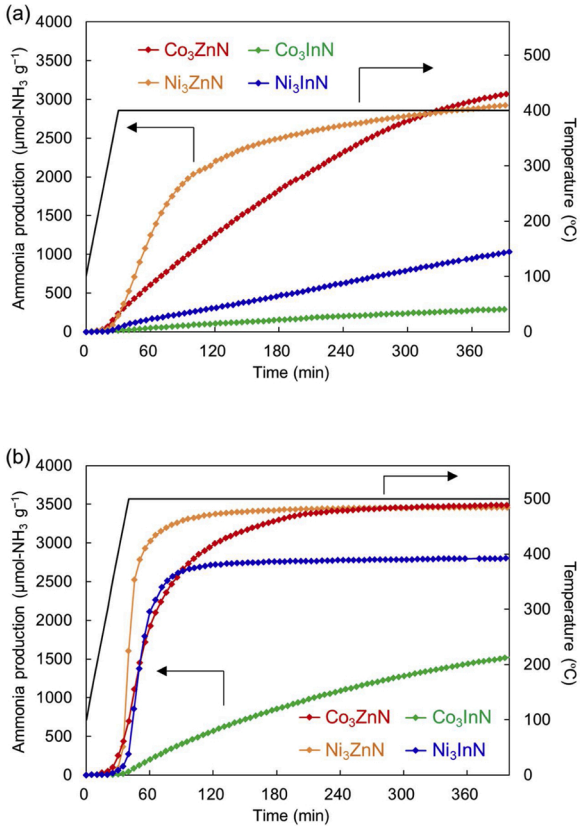

Fig. 4. Ammonia production profiles of as prepared Co_3ZnN, Ni_3ZnN, Co_3InN, and Ni_3InN under the flow of 75 % H_2/Ar at (a) 400 °C and (b) 500 °C.

Table 2
Ammonia production yields of the anti-perovskite nitrides.

compound	Ammonia production (μmol-NH_3 g^{-1})		
	Theoretical[a]	400 °C[b]	500 °C[b]
Co_3ZnN	3770	3069	3491
Ni_3ZnN	3784	2925	3461
Co_3InN	3620	289	1523
Ni_3InN	3291	1029	2804

[a] Estimated on the basis of N content in the as prepared samples.
[b] Determined from the decrease in the conductivity of the H_2SO_4 solution (0.00108 M) through which the reaction vent gas was flowed.

the reaction of the H species with lattice N atoms to form ammonia, and the desorption of the ammonia molecules are involved in ammonia production. Differences in the chemical affinities between Zn and In can be anticipated to affect these reactions resulting in the difference in the

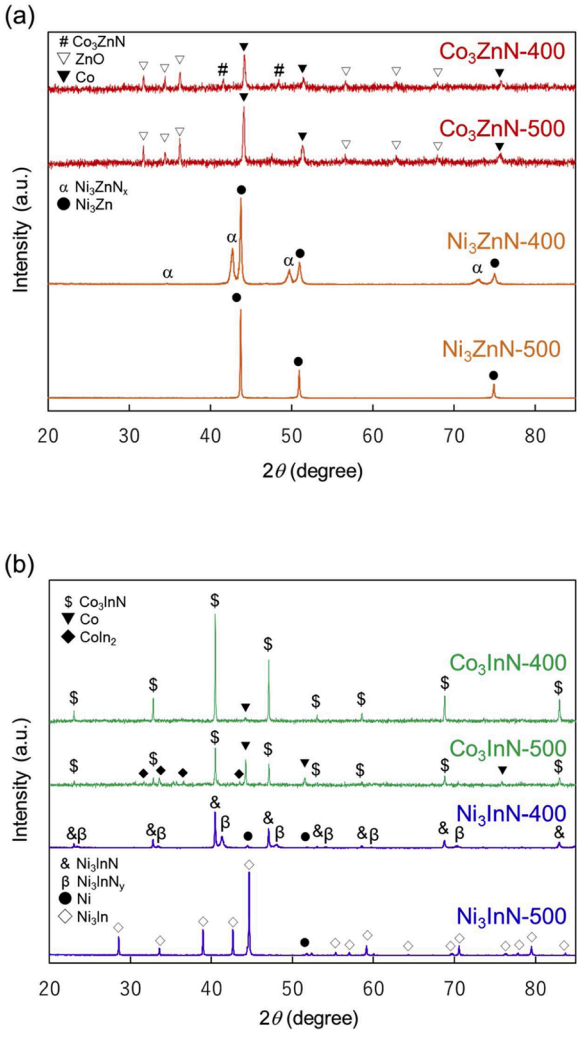

Fig. 5. XRD patterns of post-reaction samples (a) Co_3ZnN-400, Co_3ZnN-500, Ni_3ZnN-400 and Ni_3ZnN-500 and (b) Co_3InN-400, Co_3InN-500, Ni_3InN-400 and Ni_3InN-500.

ammonia production rates between Ni_3ZnN and Ni_3InN. Regarding N diffusion in the bulk, the bonding environment of N with surrounding atoms is important. In the case of Ni_3BN (B = Ga), first-principle calculations have revealed that covalent-ionic and ionic interactions occur between Ni-N and B-N, respectively [38]. The difference in the electronegativity of Zn (1.65) against N (3.04) is larger than that of In (1.78), suggesting Zn-N bonding in Ni_3ZnN to be more ionic than the In-N bonding in Ni_3InN. Moreover, the Ni-N bond distances were calculated

to be *ca.* 1.88 and 1.93 Å for Ni_3ZnN and Ni_3InN, respectively. These differences would be expected to affect the activation energy for the diffusion of N atoms. Further studies applying the Avrami-Erofe'ev relationship [39] and first-principle calculations should be undertaken to determine the dominant effect for the high ammonia release in Ni_3ZnN.

An obvious next step is to investigate the nitrogen cycling properties of these materials in which regeneration and further nitrogen discharge will be investigated. In addition, it is notable that addition of dopants including lithium in the case of manganese nitride [22], cobalt in the case of tantalum nitride [21,40] and ruthenium/alumina in the case of titanium-iron intermetallic compounds [25] have been reported to influence beneficially the lattice nitrogen conversion and/or uptake characteristics.

4. Conclusions

Anti-perovskite nitrides Co_3ZnN, Ni_3ZnN, Co_3InN, and Ni_3InN were prepared via ammonolysis using corresponding precursor oxides, and the reactivity of the N species in these nitrides was investigated using ammonia synthesis as a model reaction. All of these nitrides produced ammonia under a flow of H_2/Ar. Ni-nitrides Ni_3ZnN and Ni_3InN showed higher ammonia production rates than Co-nitrides Co_3ZnN and Co_3InN. XRD measurement indicated the existence of intermediate phases Ni_3ZnN_x and Ni_3InN_y, which could be the main factor for the higher ammonia production rates of the Ni containing systems. TGA measurements suggested regenerability for Ni_3ZnN and Ni_3InN but further experiments to substantiate this are required.

Author credit statement

YG and AD undertook the experimental work in JSJH's laboratory and under his supervision.

Declaration of Competing Interest

The authors declare that they have no known competing financial interests or personal relationships that could have appeared to influence the work reported in this paper.

Acknowledgments

We wish to express our appreciation to Professor Stuart Taylor and Miss Anna Cooper of Cardiff Catalysis Institute, School of Chemistry, Cardiff University for their very kind assistance in determining the BET surface area data reported within this manuscript. Furthermore, we are very grateful to Mr Gangi Reddy Ubbara of School of Chemistry, University of Glasgow for very kindly undertaking the combustion analyses. Angela Daisley wishes to acknowledge the EPSRC for the award of a DTA studentship (EP/N509668/1).

Appendix A. Supplementary data

Supplementary material related to this article can be found, in the online version, at doi:https://doi.org/10.1016/j.cattod.2020.03.022.

References

[1] P.H. Pfromm, Towards sustainable agriculture: fossil-free ammonia, J. Renew. Sustain. Energy. 9 (2017), 034702.
[2] R. Schlögl, Catalytic synthesis of ammonia – a never ending story? Angew. Chemie Int. Edn. 42 (2003) 2004–2008.
[3] M. Muhler, F. Rosowski, O. Hinrichsen, A. Hornung, G. Ertl, Ruthenium as a catalyst for ammonia synthesis, Stud. Surf. Sci. Catal. 101 (1996) 317–326.
[4] J. Wu, J. Li, Y. Gong, M. Kiyano, T. Inoshita, H. Hosono, Angew. Chemie Int. Edn. 58 (2019) 825–829.
[5] P. Wang, F. Chang, W. Gao, J. Guo, G. Wu, T. He, P. Chen, Nat. Chem. Biol. 9 (2017) 64–70.
[6] R. Kojima, K.-I. Aika, Cobalt molybdenum bimetallic catalysts for ammonia synthesis: part 1. Preparation and characterization, Appl. Catal. A Gen. 215 (2001) 149–160.
[7] C.J.H. Jacobsen, Novel class of ammonia synthesis catalysts, Chem. Commun. (2000) 1057–1058.
[8] S. AlSobhi, J.S.J. Hargreaves, A.L. Hector, S. Laassiri, Citrate-gel preparation and ammonia synthesis activity of compounds in the quaternary $(Ni,M)_2Mo_3N$ (M=Cu or Fe) systems, Dalton Trans. 48 (2019) 16786–16792.
[9] C.D. Zeinalipour-Yazdi, J.S.J. Hargreaves, C.R.A. Catlow, Nitrogen activation in a Mars-van Krevelen mechanism for ammonia synthesis on Co_3Mo_3N, J. Phys. Chem. C 119 (2015) 28368–28376.
[10] C.D. Zeinalipour-Yazdi, J.S.J. Hargreaves, C.R.A. Catlow, Low T mechanisms for ammonia synthesis on Co_3Mo_3N, J. Phys. Chem. C 122 (2018) 6078–6082.
[11] Y. Kobayashi, Y. Tang, T. Kageyama, H. Yamashita, N. masuda, S. Hosokawa, H. Kageyama, Titanium-based hydrides as heterogeneous catalysts for ammonia synthesis, J. Am. Chem. Soc. 139 (2017) 18240–18246.
[12] Y. Tang, Y. Kobayashi, N. Masudam, Y. Uchida, H. Okomoto, T. Kageyama, S. Hosokawa, F. Loyer, K. Mitsuhara, K. Yamanaka, Y. Tamenori, C. Tassel, T. Yamamoto, T. Tanaka, H. Kageyama, Metal-dependent support effects of oxyhydride supported Ru, Fe, Co catalysts for ammonia synthesis, Adv. Energy Mater. 8 (2018), 1801772.
[13] A.J. Medford, M.C. Hatzell, Photon-driven nitrogen fixation: current progress, thermodynamic considerations, and future outlook, ACS Catal. 7 (2017) 2624–2643.
[14] V. Kyriakou, I. Garagounis, E. Vasileiou, A. Vourros, M. Stoukides, Progress in the electrochemical synthesis of ammonia, Catal. Today 286 (2017) 2–13.
[15] M.A. Shipman, M.D. Symes, Recent progress towards the electrosynthesis of ammonia from sustainable resources, Catal. Today 286 (2017) 57–68.
[16] N. Shan, V. Chikan, P. Pfromm, B. Liu, Fe and Ni dopants facilitating ammonia synthesis on Mn_4N and mechanistic insights from first-principles methods, J. Phys. Chem. C 122 (2018) 6109–6116.
[17] R. Michalsky, P.H. Pfromm, A. Steinfeld, Rational design of metal nitride redox materials for solar-driven ammonia synthesis, Interf. Focus 5 (2015), 20140084.
[18] J.M. McEnaney, A.R. Singh, J.A. Schwalbe, J. Kibsgaard, J.C. Lin, M. Cargnello, T. F. Jaramillo, J.K. Nørskov, Ammonia synthesis from N_2 and H_2O using a lithium cycling electrification strategy at atmospheric pressure, Energ. Env. Sci. 10 (2017) 1621–1630.
[19] A.-M. Alexander, J.S.J. Hargreaves, C. Mitchell, The denitridation of nitrides of iron, cobalt and rhenium under hydrogen, Top. Catal. 56 (2013) 1963–1969.
[20] A.-M. Alexander, J.S.J. Hargreaves, C. Mitchell, The reduction of various nitrides under hydrogen: Ni_3N, Cu_3N, Zn_3N_2 and Ta_3N_5, Top, Catal. 55 (2012) 1046–1053.
[21] S. Laassiri, C.D. Zeinalipour-Yazdi, C.R.A. Catlow, J.S.J. Hargreaves, Nitrogen transfer properties in tantalum nitride based material, Catal. Today 286 (2017) 147–155.
[22] S. Laassiri, C.D. Zeinalipour-Yazdi, C.R.A. Catlow, J.S.J. Hargreaves, The potential of manganese nitride based materials as nitrogen transfer reagents for nitrogen chemical looping, Appl. Catal. B: Environ. 223 (2018) 60–66.
[23] C.D. Zeinalipour-Yazdi, J.S.J. Hargreaves, S. Laassiri, C.R.A. Catlow, The integration of experiment and computational modelling in heterogeneously catalyzed ammonia synthyesis over metal nitrides, Phys. Chem. Chem. Phys. 20 (2018) 21803–21808.
[24] D. Neagu, G. Tsekouras, D.N. Miller, H. Menard, J.T.S. Irivine, In situ growth of nanoparticles through control of non-stoichometry, Nat. Chem. Biol. 5 (2013) 916–923.
[25] M. Itoh, K.-I. Machida, K. Hirose, T. Sakata, H. Mori, G.-Y. Adachi, Nitrogenation and hydrogenation characteristics of transition metal-iron intermetallic compounds, J. Phys. Chem. B 103 (1999) 9498–9504.
[26] Y. Watanuki, S. Morii, T. Kaneko, T. Toyama, Y. Kojima, N. Nishimiya, Nitrogen absorption behaviors of ZrVFe and related alloys, J. Alloys Cpds. 731 (2018) 423–427.
[27] V. Petříček, M. Dušek, L. Palatinus, Crystallographic computing system JANA2006: general features, Z. Kristallogr. 229 (2014) 345–352.
[28] W.L. Smith, A.D. Hobson, The structure of cobalt oxide, Co_3O_4, Acta Crystallogr. B 29 (1973) 362–363.
[29] K. Krezhov, P. Konstantinov, On the cationic distribution in zinc-cobalt oxide spinels, J. Phys. Condens. Matter 5 (1993) 9287–9295.
[30] Y. Yuan, L. Yang, B. He, E. Pervaiz, Z. Shao, M. Yang, Cobalt-zinc nitride on nitrogen doped carbon black nanohybrids as a non-noble metal electrocatalyst for oxygen reduction reaction, Nanoscale 9 (2017) 6259–6263.
[31] B. He, Y. Yuan, J. Wang, E. Pervaiz, X. Dong, Z. Shao, M. Yang, Hierarchical Ni_3ZnN hollow microspheres as stable non-noble metal electrocatalysts for oxygen reduction reactions, Electrocatalysis 9 (2018) 452–458.
[32] W.H. Cao, B. He, C.Z. Liao, L.H. Yang, L.M. Zeng, C. Dong, Preparation and properties of antiperovskite-type nitrides: $InNNi_3$ and $InNCo_3$, J. Solid State Chem. 182 (2019) 3353–3357.
[33] R. Kojima, K.-I. Aika, Cobalt molybdenum bimetallic nitride catalysts for ammonia synthesis: Part 2. Kinetic study, Appl. Catal. A Gen. 218 (2001) 121–128.
[34] G.E. Hammer, R.M. Shemenski, The oxidation of zinc in air studied by XPS and AES, J. Vac. Sci. Technol. A 1 (1983) 1026–1028.
[35] R.P. Anantatmula, D.B. Masson, Thermodynamic properties of solid Ni-Zn alloys by atomic absorption, Metall. Trans. 5 (1974) 605–613.
[36] H.H. Stadelmaier, H.K. Manaktala, Intermetallic $CoIn_2$, a representative of the $CuMg_2$ structure type, Acta Cryst. B31 (1975) 374–378.
[37] E. Hellner, The system nickel-indium, Z. Metallkd. 41 (1950) 401–406.

[38] V.V. Bannikov, I.R. Shein, A.L. Ivanovskii, Structural, elastic and electronic properties of new antiperovskite-like ternary nitrides $AlNNi_3$, $GaNNi_3$ and $InNNi_3$ as predicted from first principles, Comput. Mater. Sci. 49 (2010) 457–461.
[39] J.D. Hancock, J.H. Sharp, Method of comparing solid-state kinetic data and its application to the decomposition of kaolinite, brucite, and $BaCO_3$, J. Am. Ceram. Soc. 55 (1972) 74–77.
[40] C.D. Zeinalipour-Yazdi, J.S.J. Hargreaves, S. Laassiri, C.R.A. Catlow, DFT-D3 study of H_2 and N_2 chemisorption over cobalt promoted Ta_3N_5-(100), (010) and (001) surfaces, Phys. Chem. Chem. Phys. 19 (2017) 11968–11974.